coatings

MDPI

Article

Corrosion Resistance of Waterborne Epoxy Coatings by Incorporation of Dopamine Treated Mesoporous-TiO_2 Particles

Na Wang [1,2,*], Xinlin Diao [1], Jing Zhang [1] and Ping Kang [1]

[1] Sino-Spanish Advanced Materials Institute, Shenyang University of Chemical Technology, Shenyang 110142, China; 15702426903@163.com (X.D.); zhangjingcszx@syuct.edu.cn (J.Z.); kangping@syuct.edu.cn (P.K.)

[2] Advanced Manufacturing Institute of Polymer Industry (AMIPI), Shenyang University of Chemical Technology, Shenyang 110142, China

* Correspondence: iamwangna@syuct.edu.cn; Tel.: +86-24-8938-8092

Received: 23 April 2018; Accepted: 28 May 2018; Published: 31 May 2018

Abstract: In this paper, waterborne epoxy (EP) coatings were modified by the incorporation of synthetic structure (DA/meso-TiO_2) to improve the anticorrosion ability of waterborne epoxy coatings for steel structures. Fourier transform infrared spectroscopy (FTIR), nitrogen adsorption–desorption, X-ray diffraction (XRD) and thermo-gravimetric analyses (TGA) were used to characterize textural properties of DA/meso-TiO_2. Corrosion performances of mild carbon steel coated samples were tested by salt spray tests and employing electrochemical impedance spectroscopy (EIS). FTIR, XRD, TGA and nitrogen adsorption–desorption attested to dopamine polymerization within the mesopores and on the surface of meso-TiO_2. The results of EIS and salt spray test showed that the specimen coated with 1.0 wt % DA/meso-TiO_2 exhibited optimum corrosion performance among other coating specimens.

Keywords: dopamine (DA); mesoporous-TiO_2 (meso-TiO_2); waterborne epoxy (EP); EIS

1. Introduction

Recently, waterborne epoxy resins have occupied a major place in the development of high performance light weight composites due to the unique combination of properties and are more environmentally friendly compared with epoxy resins [1–4]. Nonetheless, the primary disadvantage of waterborne epoxy resin is the formation of holes and faults over the coated surface [5–7].

Many attempts have been made to solve the problem of waterborne epoxy resins in the last few decades, such as adding other resins or antiseptic agents. However, many reports showed that nontoxic nanomaterials as fillers are the key to polish up the resistance of epoxy coating due to their small size, high surface area and high barrier properties [8]. Several papers have reported anticorrosion performance of epoxy resins were enhanced by adding small amount of nanoparticles, such as TiO_2 [9], SiO_2 [10], etc. Meso-TiO_2 not only has nanoscale size, but also has the unique pore structure compared with normal nanoparticles which could improve the anti-aging properties and barrier properties of the coating. In our previous work, we proved that waterborne epoxy resin has better anticorrosion properties due to the addition of MCM-41 and we also proved that meso-TiO_2 can increase the barrier performance of the coatings more availably due to the larger pore size of meso-TiO_2 than MCM-41 [1,11]. However, due to high surface tension of water, the compatibility between waterborne epoxy matrix and filler is poor. Therefore, to enhance compatibility between waterborne epoxy matrix and filler, meso-TiO_2 has to be modified to obtain organophilic on its surface [12,13].

In the central nervous system, dopamine is an important neurotransmitter (NT) that processes memory, regulates movement, and so on [14]. Dopamine can react with the epoxy groups as well as

interact with hydroxyl groups on the surface and in the inner-channel of meso-TiO_2 to form hydrogen bonds (Figure 1) [15,16]. The dopamine which inlays on the surface and inside of the meso-TiO_2 can strengthen possible chemical interactions between epoxy matrix and meso-TiO_2 [17], so that the molecular chain of the epoxy resin in the nano-sized pores extending along the channels to the openings, which enhance the miscibility through the entanglement and inter-diffusion between the matrix and the particulate. Meanwhile, it highly suppresses the aggregation of fillers (Figure 2) [18]. Moreover, dopamine is non-toxic and environmentally, which is suitable for non-toxic waterborne epoxy resins. Therefore, dopamine is an excellent choice to modify meso-TiO_2.

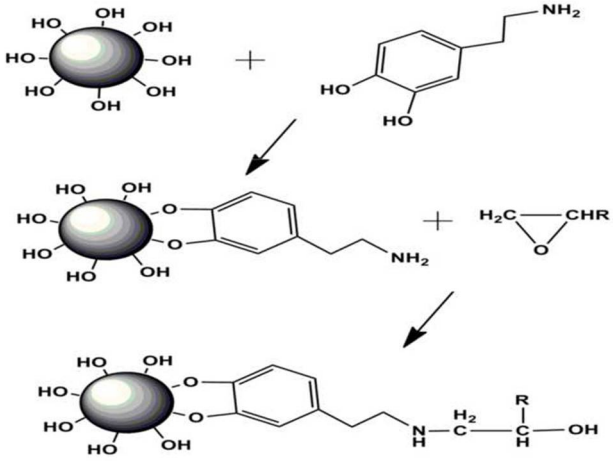

Figure 1. Mechanism of dopamine interaction with meso-TiO_2 and resin.

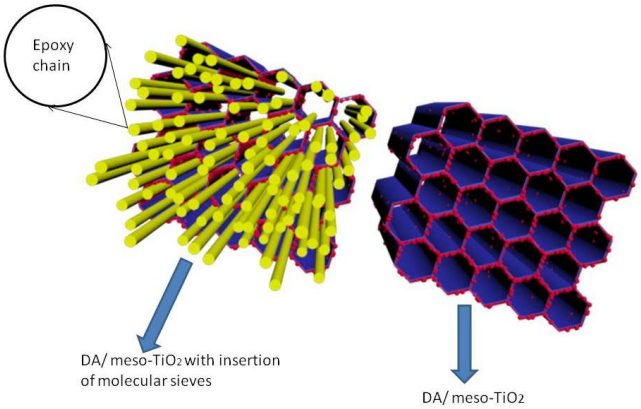

Figure 2. The schematic diagram of nanocomposite model.

In this paper, meso-TiO_2 was treated with dopamine (DA) and that was utilized as filler for waterborne epoxy resin coating to enhance compatibility between waterborne epoxy matrix and filler. The aim is to improve the compatibility of matrix with filler and enhance the chemical crosslinking to achieve better anticorrosion performance.

2. Materials and Methods

2.1. Materials

Dopamine and tris-hydroxymethylaminomethane were purchased from Sigma-Aldrich (St. Louis, MO, USA,). Waterborne epoxy resin (WSR6101) and curing agent (Anquamine 615) were purchased from Blue Star New Material Chemical Co., Ltd., Beijing, China.

2.2. Preparation of DA/meso-TiO_2

The meso-TiO_2 fillers were synthesized by our lab according to the literature [19]. In a representative procedure, 2 g of meso-TiO_2 and 2 g of dopamine were dissolved in Tris buffer solution, to which was added diluted hydrochloric acid until the pH of the solution was 8.5 and stirred at ambient temperature for 16 h. Subsequent centrifuging with distilled water three times and vacuum dried at 50 °C for at least 12 h resulted in the final DA/meso-TiO_2 nanocomposite.

2.3. Preparation of the Anticorrosion Coating

The coatings were made by taking desired quantity of filler (1.0 wt % meso-TiO_2 and 0.5 wt %, 0.7 wt %, 1.0 wt %, 2.0 wt % DA/meso-TiO_2) with waterborne epoxy resin by a pearl-mill for 30 min; afterwards, curing agent and deionized water were added into the compound and stirred by magnetic stirrers for 15 min (Table 1).

Table 1. Formulation of coatings.

Sample	Waterborne Epoxy Resin (g)	Pigment (g)	Curing Agent (g)	Water (g)
Neat epoxy	20	–	10	10
Meso-TiO_2 (1.0 wt %)	20	0.2	10	10
DA/meso-TiO_2 (0.5 wt %)	20	0.1	10	10
DA/meso-TiO_2 (0.7 wt %)	20	0.14	10	10
DA/meso-TiO_2 (1.0 wt %)	20	0.2	10	10
DA/meso-TiO_2 (2.0 wt %)	20	0.4	10	10

2.4. Preparation of the Steel Substrate

In this study, the matrix metal materials were provided by TianHua Chemical Machinery (Lanzhou, China) and Automation Research and Design Institute (Beijing, China); the type of steel is Q235A.

Steel substrates with rounded corners and edges were polished by fine emery paper, which were washed by acetone and ethanol to remove oil and water, and then dried them for next use. Then, the liquid paints (neat waterborne epoxy and waterborne epoxy nanocomposites) were applied by air spraying process and the samples were cured at room temperature for a week. Samples with the thickness of 30 ± 5 μm were tested.

2.5. Techniques and Analyses

To ascertain grafting of dopamine on the surface and inner-channels of meso-TiO_2 nanoparticles, thermo-gravimetric analyses (TGA), Fourier transform infrared spectroscopy (FTIR), N_2 adsorption–desorption and X-ray diffraction (XRD) were employed.

N_2 adsorption–desorption isotherms at 77 K were conducted on micromeritics ASAP 2010 micro-pore analysis system (Micromeritics, Norcross, GA, USA). The samples were outgassed at 473 K for 4 h.

X-ray diffraction patterns of DA/meso-TiO_2 and meso-TiO_2 were recorded on D/max-2500PC X-ray diffractometer (Rigaku, Tokyo, Japan), using Cu Kα radiation at 50 kV, a current of 200 mA, and scanning rate of 1°/min by 0.01 steps.

FTIR measurements were performed on Nicolet MNGNA-IR560 (Thermo Fisher Scientific, Waltham, MA, USA) with 4 cm^{-1} resolution for identifying the inner-channels of modified meso-TiO_2 and functional groups on the surface.

The dopamine content of meso-TiO_2 nanoparticles was tested by a thermogravimetric analyzer (NETCH STA449C, NETZSCH, Selb, Germany). The measurement was in progress under N_2 at a heating rate of 10 °C/min.

An electrochemical workstation (AUT84362, Autolab, Metrohm, Herisau, Switzerland) was used for electrochemical impedance spectroscopy (EIS) measurement on the coated specimens after exposure

to 3.5 wt % NaCl solution for 35 days. EIS measurements were performed over the frequency range of 10^{-2}–10^{5} Hz. The Autolab with ZSimpwin software (Version 3.5) was employed for analyzing the EIS data. The anticorrosion ability of the coatings was also determined by salt spray exposure (ASTM B 117 [20]).

According to the standard specified in standard ASTM B 117, the salt spray test was working in a 5% NaCl solution at 35 ± 2 °C and 100% relative humidity. Coatings with 30 ± 5 um thickness were used for salt spray exposure and the salt spray was sprayed for 1 min every 6 min. After 600 h, the specimens were taken out from the salt spray chamber and the representative areas were imaged by a digital camera for evaluating corrosion performance of the coated specimens.

3. Results and Discussion

3.1. FTIR Results

FTIR spectroscopy was used to determine dopamine grafting onto the surface and inner-channel of meso-TiO_2 [21,22]. Figure 3 shows FT-IR spectra of: (a) meso-TiO_2; and (b) DA/meso-TiO_2. In Figure 3a, the absorption at 3370 cm^{-1} suggested the characteristic peaks of –OH bonds present in meso-TiO_2 structures, and the broad and strong adsorption band at 850 cm^{-1} in the spectrum corresponded to Ti–O–Ti stretching vibrations [23,24]. By comparing FTIR spectra of DA/meso-TiO_2 with pure meso-TiO_2, a change in intensity of peaks was observed (Figure 3a,b), the increase in intensity of bands at 3500 and 3300 cm^{-1} suggesting that free –OH groups were affected by –NH– bonds present in dopamine (Figure 3b). In addition, the adsorption bands at 1291 cm^{-1} was caused by the asymmetric bending vibration of C–O–H band. These results confirmed that meso-TiO_2 was exactly modified by dopamine.

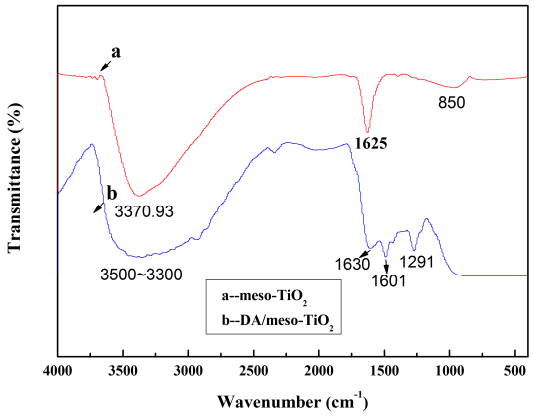

Figure 3. FTIR spectra of (**a**) meso-TiO_2 and (**b**) DA/meso-TiO_2.

3.2. Nitrogen Adsorption–Desorption Results

Figure 4 shows the corresponding pore size distribution curve and nitrogen adsorption–desorption isotherms obtained from the desorption branch of the nitrogen isotherm of meso-TiO_2 and DA/meso-TiO_2. The isotherm of meso-TiO_2 was observed as classical Type IV, typical of mesoporous solids. Moreover, H1 hysteresis loop implied that meso-TiO_2 had a unique pore structure [25]. The various parameters of mesoporous samples are shown in Table 2.

The BJH (aperture distribution test) analyses showed that meso-TiO_2 exhibited an average pore-size of about 5.8 nm calculated from the desorption branch of the nitrogen adsorption isotherm [1]. Table 2 shows that the pore volume of modified with dopamine decreased from 0.235 to 0.074 $mL \cdot g^{-1}$ compared with the pore volume of meso-TiO_2. There was a starting point of hysteresis loop observed after the P/P_0 = 0.85, as shown in Figure 4, which might be caused by the particles accumulated in

hole on the surface of meso-TiO_2. Nitrogen adsorption–desorption isotherm studies further illustrated that dopamine was successfully grafted onto the inner-channel and surface of meso-TiO_2.

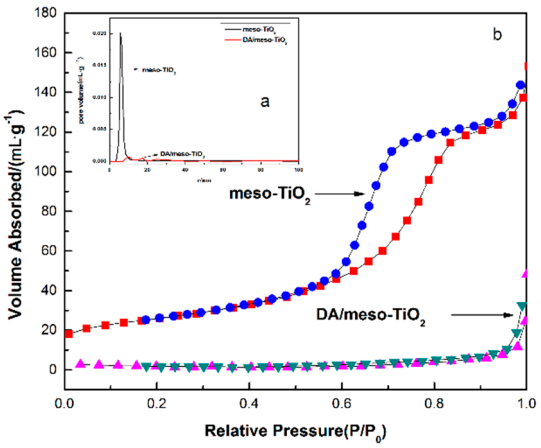

Figure 4. (**a**) The corresponding pore size distribution curve and (**b**) nitrogen adsorption–desorption isotherms obtained from the desorption branch of the nitrogen isotherm of meso-TiO_2 and DA/meso-TiO_2.

Table 2. The results of nitrogen adsorption–desorption.

Samples	Average Pore-Size (nm)	BET ($m^2 \cdot g^{-1}$)	Pore Volume ($mL \cdot g^{-1}$)
meso-TiO_2	5.8	94.43	0.253
DA/meso-TiO_2	4.7	9.84	0.074

3.3. X-ray Diffraction Results

The powder XRD patterns of meso-TiO_2 and DA/meso-TiO_2 are shown in Figure 5. The appearance of peaks at (101), (004), (200) and (211) (Figure 5a,b), which elucidated that these particles owned crystal (anatase) [26]. Nevertheless, different samples showed differences in their peak intensities. The shape and position, which correspond to the crystal peaks of the two curves in Figure 5, are basically alike, illustrating that, before and after modifying with DA, there was no obvious change in the crystal structure of meso-TiO_2. The XRD peaks of DA/meso-TiO_2 exhibit significant peak broadening indicates that particle size of meso-TiO_2 decreased with the introduction of DA. All the above results showed that the treatment method did not alter the crystal structure of meso-TiO_2.

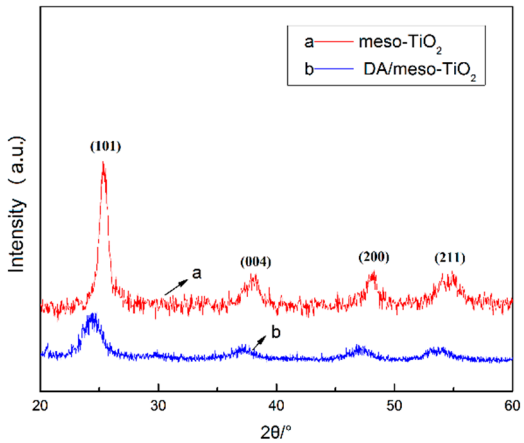

Figure 5. XRD patterns of the specimens: (**a**) meso-TiO_2 and (**b**) DA/meso-TiO_2.

3.4. Thermo-Gravimetric Analyses (TGA)

The weight loss obtained for meso-TiO_2 and modified meso-TiO_2 are shown in Figure 6. As exhibited in Figure 6a, the thermal degradation process of the meso-TiO_2 was in two stages: the slight weight loss observed below 150 °C was attributed to the elimination of physisorbed water; and the weight loss between 150 and 700 °C was attributed to the dissociation of water and the hydroxyl group on the surface of meso-TiO_2. As shown in Figure 6b, the thermal degradation process of DA/meso-TiO_2 and meso-TiO_2 was comparatively similar in earlier stage. In contrast, the maximum mass loss rate of DA/meso-TiO_2 was higher compared with meso-TiO_2. It can be attributed to the chemical interaction between DA and meso-TiO_2. It was revealed by TGA measurement that dopamine was adsorbed into the pore channel and on the surface of meso-TiO_2.

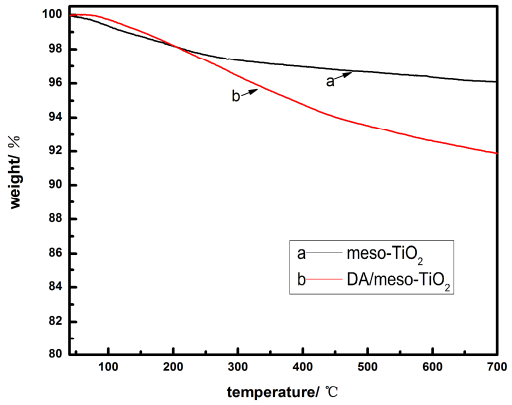

Figure 6. TGA curves of (**a**) meso-TiO_2 and (**b**) DA/meso-TiO_2.

3.5. Electrochemical Impedance Spectroscopy (EIS)

The Nyquist plots obtained from EIS measurements for coated mild steel samples which were immersed in 3.5 wt % NaCl solution for 820 h are exhibited in Figure 7. In the overall structure shown in Figure 7, the diameter of capacitance arc is in proportion to impedance modulus [27,28].

In Figure 7a, at the early stage of immersion (0 h), the coating resistance in the low frequency was higher than 2.25×10^7 $\Omega \cdot cm^2$ for neat epoxy coating. With the increase of soaking time (360 h), the impedance value decreased sharply, the electrolyte solutions easily penetrated to the interface of matrix and coating through the micropores of the coating surface. At this stage, the rate at which the electrolyte solution entered the coating from the coating channel was much less than the rate at which the electrolyte generated corrosion products at the interface, the process of corrosion was affected by the diffusion of corrosion products into the solution. With further increasing immersion time (720 h), the barrier properties of coating appeared to rise again due to the formation of corrosion products on the substrate surface, which formed a passivation film. Ultimately, as soaking time increases to 820 h, the impedance of the coating decreased again. It could be attributed to the electrolyte solution penetrating the coating, the pore size of the coating increasing and the passivation film being destroyed by chloride ions. At this time, the corrosion process was accelerated due to the process of charge transfer [29,30].

For the epoxy coating containing meso-TiO_2 (Figure 7b), it indicated that the spectra of the coating with meso-TiO_2 showed distinct difference from that of the varnish coating, the barrier property of coatings was generally illustrated by the radius of measured capacitive semi-circle and the barrier ability of the coatings was positively correlated with the radius of measured semicircle of the capacitance [31]. The radius of the capacitive semi-circle of the coating with meso-TiO_2 was larger compared to the radius of capacitive semi-circle obtained from neat epoxy coating. Therefore, the anticorrosion property of the coating containing meso-TiO_2 was better than pure

epoxy coating. It showed that the addition of meso-TiO_2 could improve the barrier ability of epoxy resin coating effectively.

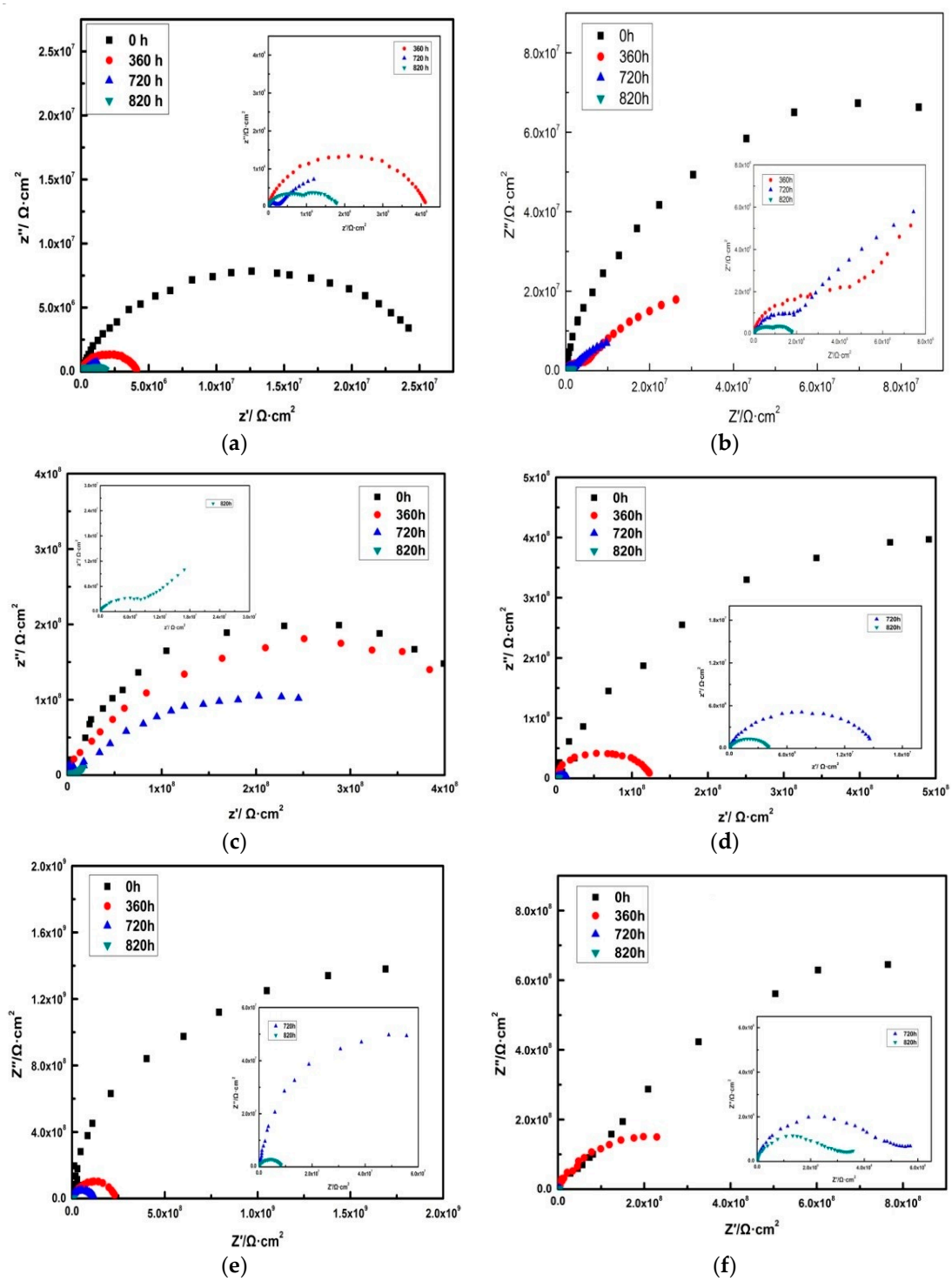

Figure 7. Nyquist diagrams of the six coatings in different immersiontime: (**a**) pure epoxy coating; (**b**) 1.0% meso-TiO_2 coating; (**c**) 0.5% DA/meso-TiO_2 coating; (**d**) 0.7% DA/meso-TiO_2 coating; (**e**) 1.0% DA/meso-TiO_2 coating; and (**f**) 2.0% DA/meso-TiO_2 coating.

For the coatings containing DA/meso-TiO_2 (Figure 7c–f), in the same immersion time, the radius of capacitive semi-circle of the coating containing DA/meso-TiO_2 was higher compared with pure

epoxy coating and the coating with meso-TiO_2. Therefore, the barrier ability of the coatings with DA/meso-TiO_2 was better than the coating containing meso-TiO_2. It proved that dopamine can effectively improve the compatibility between the meso-TiO_2 and waterborne epoxy resin. Then, the resistance value for all coatings gradually decreased by increasing the immersion time. In Figure 7d, it is clear that the coating containing DA/meso-TiO_2 (0.5%) had two semicircles, which implied that there were two time constants. For the other epoxy coatings (0.7%, 1.0% and 2.0%), only one apparent time constant was observed, but the resistance values of coating containing DA/meso-TiO_2 (1.0%) were much higher than those of coating with DA/meso-TiO_2 (0.7% and 2.0%). These results showed that the coating containing DA/meso-TiO_2 (1.0%) had the best barrier ability than other three coatings.

To make clear the corrosion resistance of different samples at different times, equivalent circuit models were used to fit EIS results, as shown in Figure 8 [32]. In Figure 8a, R_s, Q_c and R_{ct} represent the solution resistance, coating capacitance and coating resistance, respectively [33]. In the initial immersion, the corrosive ions cannot penetrate the coatings because waterborne epoxy coatings had good barrier abilities and the waterborne epoxy coatings were equivalent to capacitors. In Figure 8b, R_p and R_{dl} represent polarization resistance and capacity of double layer, respectively. Figure 8c shows the model to fit Nyquist data of the process (820 h), and W represents diffusion resistance. With increasing immersion time, the corrosive ions penetrated the coatings through artificial defects and natural pores on the surface of the coatings. The W appeared because the corrosive ions diffused into the solution in this process.

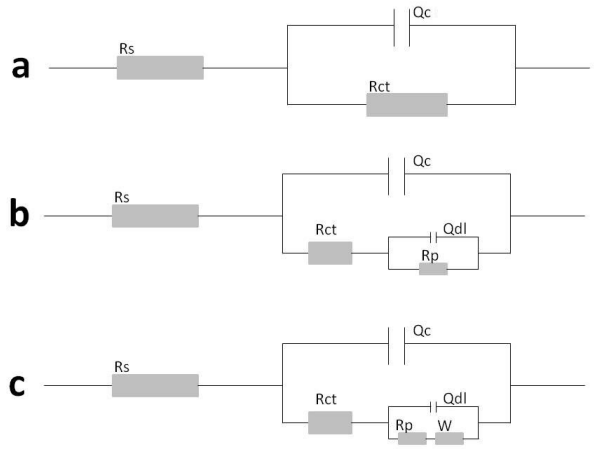

Figure 8. Equivalent electrical circuits.

The EIS Bode plots are shown in Figure 9; the resistance value of neat coating was minimum at high frequency range or low frequency range, compared with others. It indicated that all the stuffing played a certain role in blocking the coating microholes. The differences in impedance (Z) of the same frequency range indicated that the passage of corrosive ions to the metal surface through the coating was impeded, which was due to an improved interfacial barrier in the presence of those additives [34]. For the epoxy coating with fillers, the impedance of the coatings containing 1.0 wt % DA/meso-TiO_2 was higher than the coating containing 1.0 wt %meso-TiO_2 over the entire frequency range. It suggested that meso-TiO_2 was modified by dopamine that can effectively improve the corrosion resistance of the coatings.

For the coatings containing DA/meso-TiO_2, the corrosion resistance of the coatings would be different with different amounts of fillers. It can be found that, among the specimens (Figure 9d), the curve of the coating resistance with 0.5 wt % DA/meso-TiO_2 had the best value in both high frequency and low frequency areas. However, comparing Figure 7c (820 h) and Figure 7e (820 h), it is not difficult to find that coating with 0.5 wt % DA/meso-TiO_2 presented Warburg impedance, which means that corrosion medium entered the interior of the coating and the coating began to lose its

anticorrosion ability. Thus, as we can see from the specimens (Figure 9a–d), the coating resistance with 1.0 wt % DA/meso-TiO_2 was the best at all frequency region, which indicated that the addition of 1.0 wt % DA/meso-TiO_2 was the most appropriate.

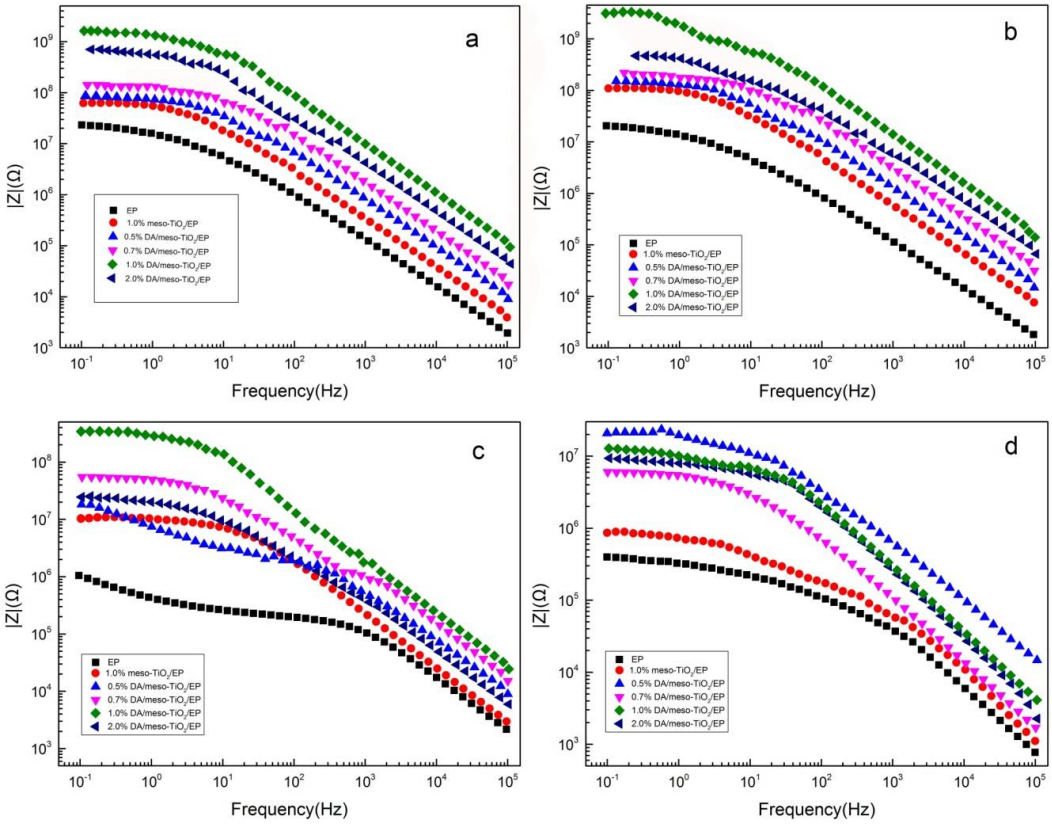

Figure 9. Bode magnitude plots of the samples immersed in 3.5% NaCl solution for various times: (**a**) 0 h; (**b**) 360 h; (**c**) 720 h; and (**d**) 820 h.

Figure 10 shows the Schematic models of mechanism of: (a) neat waterborne epoxy coating; (b) waterborne epoxy coating containing meso-TiO_2; and (c) waterborne epoxy coating containing DA/meso-TiO_2.

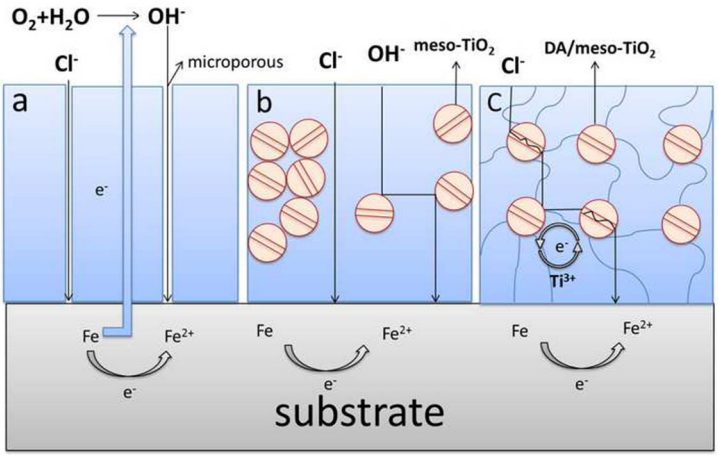

Figure 10. The simulation of anticorrosion mechanism: (**a**) neat waterborne epoxy coating; (**b**) waterborne epoxy coating containing meso-TiO_2; and (**c**) waterborne epoxy coating containing DA/meso-TiO_2.

Figure 10a shows that the steps of rust formation on matrix required continuous charge transfer. If the processes were prevented or delayed, the corrosion will be inhibited and the coating becomes effective for corrosion prevention [1]. Firstly, from the point of view of the electrochemical structure, the composite coating modified by DA/meso-TiO_2 would include the elements of S and Ti, in which there were some empty or not full d orbitals. The combination of d orbitals with Fe^{2+} could generate the feedback π bond and then make the d electronic on Fe feedback to the elements, which could reduce the electron cloud density of Fe element [35]. With increasing immersion time, a passivation film was formed due to the accumulation of corrosion products on the surface of matrix and the transportation of the electron was prevented. In aqueous solution, dopamine was easily oxidized to self-polymerize to form cross-linked structures on the inner-channel and surface of meso-TiO_2, which could obviously improve the binding strength between coating and matrix and the density of coating. Thus, the transport process of the electronics was affected and then the electrochemical corrosion process was delayed. It indicated that the transmission channel of the corrosive medium was inhibited which could increase the anticorrosion ability of the epoxy coating.

3.6. Salt Spray Test

Moreover, the anticorrosion durability performance of coating samples without artificial defects was tested. Figure 11 exhibits the salt spray test results of the coating specimens after 600 h exposure. In the case of neat epoxy coating, serious rusting appeared along the surface. In other words, the rate of corrosion for neat epoxy coating was the fastest (Figure 11a). The sample of the coating containing meso-TiO_2 also had little rust. The amount of rust was less compared with the sample of neat epoxy coating (Figure 11b). It further manifested that the anticorrosion ability of epoxy coatings enhanced due to addition of nanoparticles to epoxy coating. The sample of the coatings containing DA/meso-TiO_2 had less rust compared with the other two coatings (Figure 11a,b). The modified meso-TiO_2 with dopamine considerably improved the corrosion protection properties of epoxy coating, compared to unmodified meso-TiO_2. It showed the coating with the addition of 1.0 wt % DA/meso-TiO_2 had the least rust. The results indicate that the addition of 1.0 wt % DA/meso-TiO_2 could effectively suppress the occurrence and propagation of localized corrosion under harsh conditions, which was consistent with the results of EIS analysis.

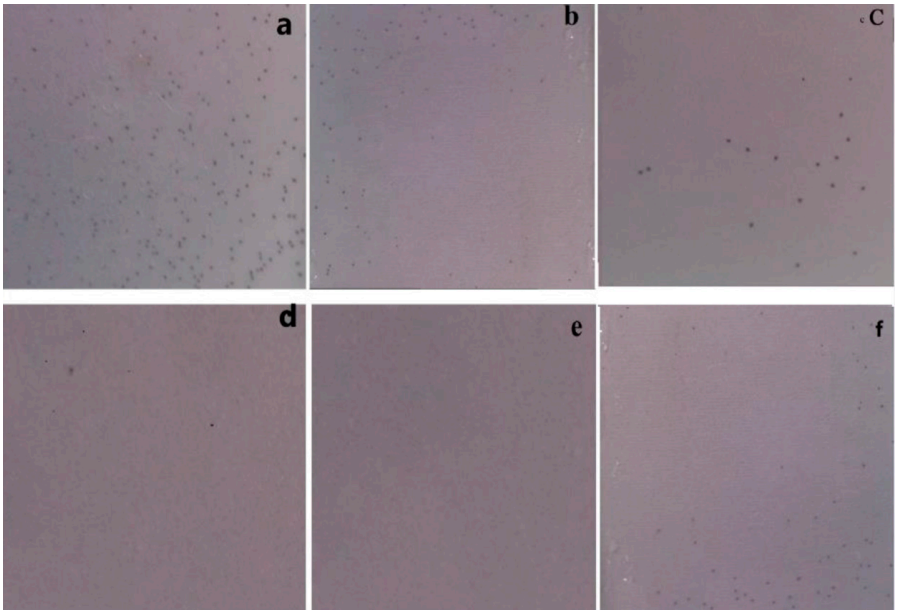

Figure 11. Surface appearance of the coatings after salt spray testing for 600 h: (**a**) neat epoxy coating; (**b**) 1.0% meso-TiO_2 coating; (**c**) 0.5% DA/meso-TiO_2 coating; (**d**) 0.7% DA/meso-TiO_2 coating; (**e**) 1.0% DA/meso-TiO_2 coating; and (**f**) 2.0% DA/meso-TiO_2 coating.

4. Conclusions

The anticorrosion ability of the epoxy coating containing unmodified and modified meso-TiO_2 with dopamine on steel substrate was investigated. According to our studies, the following conclusions can be made.

FTIR and XRD results showed that meso-TiO_2 was obtained successfully. The results of FTIR, TGA and Nitrogen adsorption–desorption confirmed that dopamine was successfully grafted onto the surface and inner-channel of meso-TiO_2. The XRD results also showed that the crystal structure was not altered after the modification of meso-TiO_2 with dopamine. EIS and salt spray test results revealed that inclusion of unmodified nanoparticles in the epoxy coating increased the corrosion resistance compared to the pure epoxy coating and the DA/meso-TiO_2 (1.0 wt %) significantly improved the corrosion resistance of the waterborne epoxy varnish via increasing barrier properties. In addition, the unique properties of dopamine ensured a unique network structure was formed between the dopamine and the epoxy groups, resulting in a significant increase in the barrier properties of the coatings.

Author Contributions: N.W. and X.D. conceived and designed the experiments; N.W. and X.D. performed the experiments; J.Z. and P.K. helped to get the data through the operating instrument (e.g., the Nicolet MNGNA-IR560, the D/max-2500PC X-ray diffractometer, the scanning electron microscope); and N.W. and X.D. wrote the paper.

Funding: This research was funded by the Finance Refers to Top Talents of Liaoning Province (Grant No. [2016]864); the BaiQianWan Talents Program of Liaoning Province (Grant No. [2017]62); Innovative Talents Program of Universities in Liaoning Province (Grant No. [2017]053); International cooperation project, Shenyang Municipal Science and Technology Bureau (Grant No. 17-51-6-00); Technological Innovation Talents Program for Youngs and Middles of Shenyang, Shenyang Municipal Science and Technology Bureau (Grant No. RC170118) and Sino-Spanish Advanced Materials Institute, Shenyang Municipal Science and Technology Bureau (Grant No. 18-005-6-04).

Conflicts of Interest: The authors declare no conflict of interest.

References

1. Wang, N.; Wu, H.; Cheng, Q. Investigation on anticorrosion performance of polyaniline-mesoporous MCM-41 composites in new water-based epoxy coating. *Mater. Corros.* **2015**, *65*, 968–976. [CrossRef]
2. Liu, D.; Zhao, W.; Liu, S. Comparative tribological and corrosion resistance properties of epoxy composite coatings reinforced with functionalized fullerene C60 and graphene. *Surf. Coat. Technol.* **2016**, *286*, 354–364. [CrossRef]
3. Guadagno, L.; Raimondo, M.; Vittoria, V. Development of epoxy mixtures for application in aeronautics and aerospace. *RSC Adv.* **2014**, *4*, 485–494. [CrossRef]
4. Pourhashem, S.; Rashidi, A.; Vaezi, R. Excellent corrosion protection performance of epoxy composite coatings filled with amino-silane functionalized graphene oxide. *Surf. Coat. Technol.* **2017**, *317*, 1–9. [CrossRef]
5. Chen, Z.H.; Tang, Y.; Yu, F. Preparation of light color antistatic and anticorrosive waterborne epoxy coating for oil tanks. *J. Coat. Technol. Res.* **2008**, *5*, 259–269. [CrossRef]
6. Li, Z.; Young, R.J.; Wang, R. The role of functional groups on graphene oxide in epoxy nanocomposites. *Polymer* **2013**, *54*, 5821–5829. [CrossRef]
7. Dhoke, S.K.; Khanna, A.S. Electrochemical behavior of nano-iron oxide modified alkyd based waterborne coatings. *Mater. Chem. Phys.* **2009**, *117*, 550–556. [CrossRef]
8. Nematollahi, M.; Heidarian, M.; Peikari, M. Comparison between the effect of nanoglass flake and montmorillonite organoclay on corrosion performance of epoxy coating. *Corros. Sci.* **2010**, *52*, 1809–1817. [CrossRef]
9. Yu, Z.; Di, H.; Ma, Y. Preparation of graphene oxide modified by titanium dioxide to enhance the anti-corrosion performance of epoxy coatings. *Surf. Coat. Technol.* **2015**, *276*, 471–478. [CrossRef]
10. Pourhashem, S.; Vaezi, M.R.; Rashidi, A. Investigating the effect of SiO_2-graphene oxide hybrid as inorganic nanofiller on corrosion protection properties of epoxy coatings. *Surf. Coat. Technol.* **2017**, *311*, 282–294. [CrossRef]

11. Wang, N.; Cheng, K.; Wu, H. Effect of nano-sized mesoporous silica MCM-41 and MMT on corrosion properties of epoxy coating. *Prog. Org. Coat.* **2012**, *75*, 386–391. [CrossRef]
12. Mallakpour, S.; Barati, A. Efficient preparation of hybrid nanocomposite coatings based on poly(vinyl alcohol) and silane coupling agent modified TiO_2 nanoparticles. *Prog. Org. Coat.* **2011**, *71*, 391–398. [CrossRef]
13. Salami-Kalajahi, M.; Haddadi-Asl, V.; Rahimi-Razin, S. Investigating the effect of pristine and modified silica nanoparticles on the kinetics of methyl methacrylate polymerization. *Chem. Eng. J.* **2011**, *174*, 368–375. [CrossRef]
14. Derkach, K.V.; Romanova, I.V.; Shpakov, A.O. Functional interaction between the dopamine and melanocortin systems of the brain. *Neurosci. Behav. Physiol.* **2018**, *48*, 213–219. [CrossRef]
15. Hu, Y.R.; Guo, C.; Wang, F. Improvement of microalgae harvesting by magnetic nanocomposites coated with polyethylenimine. *Chem. Eng. J.* **2014**, *242*, 341–347. [CrossRef]
16. Sbirrazzuoli, N.; Mititelu-Mija, A.; Vincent, L. Isoconversional kinetic analysis of stoichiometric and off-stoichiometric epoxy-amine cures. *Thermochim. Acta* **2006**, *447*, 167–177. [CrossRef]
17. Wang, N.; Fu, W.; Zhang, J. Corrosion performance of waterborne epoxy coatings containing polyethylenimine treated mesoporous-TiO_2 nanoparticles on mild steel. *Prog. Org. Coat.* **2015**, *89*, 114–122. [CrossRef]
18. Wang, N.; Fang, Q.; Zhang, J. Incorporation of nano-sized mesoporous MCM-41 material used as fillers in natural rubber composite. *Mater. Sci. Eng. A* **2011**, *528*, 3321–3325. [CrossRef]
19. Hou, W.; Xiao, Y.; Han, G. Preparation of mesoporous titanium dioxide anode by a film- and pore-forming agent for the dye-sensitized solar cell. *Mater. Res. Bull.* **2016**, *76*, 140–146. [CrossRef]
20. *ASTM B117-03 Standard Practice for Operating Salt Spray (Fog) Apparatus*; ASTM International: West Conshohocken, PA, USA, 2003.
21. Wang, N.; Zhang, Y.; Chen, J. Dopamine modified metal-organic frameworks on anti-corrosion properties of waterborne epoxy coatings. *Prog. Org. Coat.* **2017**, *109*, 126–134. [CrossRef]
22. Haddadi, S.A.; Mahdavian, M.; Karimi, E. Evaluation of corrosion protection properties of epoxy coating containing sol-gel surface modified nano-zirconia on mild steel. *RSC Adv.* **2015**, *5*, 28769–28777. [CrossRef]
23. Ko, Y.I.; Kim, B.S.; Bae, J.S. Silicone-coated elastomeric polylactide nanofiber filaments: Mechanical properties and shape memory behavior. *RSC Adv.* **2013**, *3*, 20091–20098. [CrossRef]
24. Francis, B.; Thomas, S.; Jose, J. Hydroxyl terminated poly(ether ether ketone) with pendent methyl group toughened epoxy resin: Miscibility, morphology and mechanical properties. *Polymer* **2005**, *46*, 12372–12385. [CrossRef]
25. Venkatachalam, N.; Palanichamy, M.; Arabindoo, B. Enhanced photocatalytic degradation of 4-chlorophenol by Zr^{4+} doped nano TiO_2. *J. Mol. Catal. A Chem.* **2007**, *266*, 158–165. [CrossRef]
26. Irala, D.R.; Fontana, L.C.; Sagás, J.C. The effects of plasma nitriding pretreatment in steel substrates on the photocatalytic activity of TiO_2 films. *Surf. Coat. Technol.* **2014**, *240*, 154–159. [CrossRef]
27. Zhang, J.T.; Hu, J.M.; Zhang, J.Q. Studies of water transport behavior and impedance models of epoxy-coated metals in NaCl solution by EIS. *Prog. Org. Coat.* **2004**, *51*, 145–151. [CrossRef]
28. Shinde, V.P. Study of water transport characteristics of poly(*o*-ethylaniline) coatings: Corrosion mechanism. *Ionics* **2018**, *24*, 605–615. [CrossRef]
29. Chen, Y.; Hong, T.; Gopal, M. EIS studies of a corrosion inhibitor behavior under multiphase flow conditions. *Corros. Sci.* **2000**, *42*, 979–990. [CrossRef]
30. Yang, X.K.; Li, Q.; Zhang, S.Y. Electrochemical corrosion behaviors and protective properties of Ni–Co–TiO_2 composite coating prepared on sintered NdFeB magnet. *J. Solid State Electrochem.* **2010**, *14*, 1601–1608. [CrossRef]
31. Scully, J.R. Electrochemical impedance of organic-coated steel: Correlation of impedance parameters with long-term coating deterioration. *J. Electrochem. Soc.* **1989**, *136*, 979–990. [CrossRef]
32. Liu, B.; Du, P.; Zhao, C.; Wang, P. Synthesis of L-histidine-attached graphene nanomaterials and their application for steel protection. *Appl. Nano Mater.* **2018**, *1*, 1385–1395. [CrossRef]
33. Zhang, Y.; Yu, P.; Wu, J. Enhancement of anticorrosion protection via inhibitor-loaded ZnAlCe-LDH nanocontainers embedded in sol-gel coatings. *J. Coat. Technol. Res.* **2018**, *15*, 303–313. [CrossRef]

34. Wang, P.; Zhang, D.; Qiu, R. Green approach to fabrication of a super-hydrophobic film on copper and the consequent corrosion resistance. *Corros. Sci.* **2014**, *80*, 366–373. [CrossRef]
35. Eduok, U.; Suleiman, R.; Gittens, J. Anticorrosion/antifouling properties of bacterial spore-loaded sol-gel type coating for mild steel in saline marine condition: A case of thermophilic strain of *Bacillus licheniformis*. *RSC Adv.* **2015**, *5*, 93818–93830. [CrossRef]